

1 **Response of Northern Hemisphere**
2 **Midlatitude Circulation to Arctic**
3 **Amplification in a Simple Atmospheric**
4 **General Circulation Model**

5 YUTIAN WU *

Department of Earth, Atmospheric and Planetary Sciences, Purdue University

KAREN L. SMITH

Lamont-Doherty Earth Observatory of Columbia University

Submitted to J. Clim. on August 24, 2015

Revision Submitted on December 8, 2015

Accepted on January 07, 2016

* *Corresponding author address:* Yutian Wu, Department of Earth, Atmospheric, and Planetary Sciences,
Purdue University, West Lafayette, IN, 47907

E-mail: wu640@purdue.edu

ABSTRACT

7 This study examines the Northern Hemisphere midlatitude circulation response to Arctic
8 Amplification (AA) in a simple atmospheric general circulation model. It is found that, in
9 response to AA, the tropospheric jet shifts equatorward and the stratospheric polar vortex
10 weakens, robustly for various AA forcing strengths. Despite this, no statistically significant
11 change in the frequency of sudden stratospheric warming events is identified.

12 In addition, in order to quantitatively assess the role of stratosphere-troposphere coupling,
13 the tropospheric pathway is isolated by nudging the stratospheric zonal mean state towards
14 the reference state. When the nudging is applied, rendering the stratosphere inactive, the
15 tropospheric jet still shifts equatorward, but by approximately half the magnitude compared
16 to that of an active stratosphere. The difference represents the stratospheric pathway and the
17 downward influence of the stratosphere on the troposphere. This suggests that stratosphere-
18 troposphere coupling plays a non-negligible role in establishing the midlatitude circulation
19 response to AA.

20 1. Introduction

21 The Arctic has experienced a large near-surface warming trend during the past few
22 decades, about twice as large as the global average, and this is widely known as 'Arctic
23 Amplification' (AA). As a consequence of increasing anthropogenic greenhouse gases, state-
24 of-the-art climate models have consistently suggested a further warming of the Arctic, which
25 is again about two times the global average warming in the annual mean at the end of
26 the 21st century (see Collins et al. 2013). Projected AA peaks in early winter (November-
27 December) and has a consistent vertical structure that exhibits the largest warming near
28 the surface extending to the mid-troposphere. It is likely that AA is caused by a mixture
29 of mechanisms, not only limited to sea ice and snow albedo feedback, but also longwave
30 radiation feedback, lapse rate feedback, increased moisture transport and increased oceanic
31 transport (references in Collins et al. 2013; Pithan and Mauritsen 2014).

32 There is an increasing body of observational and modeling evidence that AA might
33 strongly impact both the weather and climate, not only in the Arctic region, but also remotely
34 in the Northern Hemisphere (NH) midlatitudes (see review articles by Cohen et al. 2014
35 and Barnes and Screen 2015 and references therein). In general, most of these studies
36 have detected an atmospheric circulation response resembling a negative North Atlantic
37 Oscillation (NAO) or Northern Annular Mode (NAM) pattern as a result of sea ice decline
38 and accompanied AA. However, discrepancies in the atmospheric circulation response exist
39 among different model integrations. For example, Screen et al. (2013) used two independent
40 atmospheric general circulation models (AGCM) forced with identical sea ice loss and found
41 large disagreement on the timing and magnitude of the response.

42 The adjustment of atmospheric circulation to sea ice loss has been studied extensively,
43 with the primary focus on the tropospheric pathway. It was found that transient eddy feed-
44 backs play an important role in shaping the circulation response in equilibrium and that they
45 significantly contribute to the transition from the initial baroclinic response into an equiva-
46 lent barotropic response with enhanced magnitude and spatial extent (e.g., Deser et al. 2004

47 and references therein). Besides the tropospheric pathway, Cohen et al. (2014) and Barnes
48 and Screen (2015) suggested that a stratospheric pathway may also be an important mecha-
49 nism by which AA could modify the midlatitude circulation. The stratospheric pathway has
50 received greater attention lately yet is not fully understood. An example of the stratospheric
51 pathway linking cryospheric variability and the NAM is the observed and simulated connec-
52 tion between October Eurasian snow cover and midlatitude surface weather conditions in
53 winter (Cohen et al. 2007; Fletcher et al. 2009; Cohen et al. 2010; Smith et al. 2010). The
54 mechanism involves a two-way stratosphere-troposphere interaction: a snow-forced plane-
55 tary wave anomaly propagates upward from the troposphere into the stratosphere, primarily
56 due to linear constructive interference (when the wave anomaly is in phase with the climatol-
57 ogy), and drives a weakening of the stratospheric polar vortex. The stratospheric circulation
58 anomaly later propagates downward back into the troposphere after weeks to months, result-
59 ing in a negative NAM pattern near the surface. As a consequence of AA and the possible
60 increase in planetary-scale wave activity (e.g., Peings and Magnusdottir 2014; Feldstein and
61 Lee 2014; Kim et al. 2014; Sun et al. 2015), we expect a similar stratosphere-troposphere
62 coupling to connect AA with the NH midlatitude circulation anomalies. However, previous
63 studies do not even agree on the stratospheric circulation response - some modeling stud-
64 ies reported a strengthened stratospheric polar vortex (e.g., Scinocca et al. 2009; Cai et al.
65 2012; Screen et al. 2013; Sun et al. 2014) whereas others found a weakening (e.g., Peings and
66 Magnusdottir 2014; Feldstein and Lee 2014; Kim et al. 2014), followed by a negative NAM
67 anomaly in the troposphere and near the surface.

68 In particular, recent studies of Sun et al. (2014, 2015) conducted identical prescribed sea
69 ice loss experiments with a pair of 'low-top' (poorly-resolved stratosphere) and 'high-top'
70 (well-resolved stratosphere) AGCMs - Community Atmospheric Model version 4 (CAM4)
71 and Whole Atmosphere Community Climate Model version 4 (WACCM4). Both CAM4 and
72 WACCM4 are developed at the National Center for Atmospheric Research (NCAR) and
73 have identical horizontal resolution and physics (except for gravity wave parameterization

74 and surface wind stress parameterization); however, their vertical extensions are vastly dif-
75 ferent (~ 45 km versus ~ 140 km). Sun et al. (2014, 2015) found that the negative NAM
76 response in the troposphere in WACCM4 is qualitatively similar to that in CAM4 but is
77 statistically significantly stronger. The difference between WACCM4 and CAM4 appears
78 as a downward migrating signal from the stratosphere to the troposphere. However, due to
79 several other factors that may play a role such as different climatological mean states be-
80 tween the 'low-top' and 'high-top' models, Sun et al. (2014, 2015) could not make a definite
81 conclusion on the importance of the stratospheric pathway. In addition, Sun et al. (2015)
82 explicitly demonstrated that the stratospheric circulation response could be sensitive to the
83 geographical locations of Arctic sea ice loss. When the AGCM was forced with the sea ice
84 loss within the Arctic Circle, mostly over the Barents-Kara sea (B-K sea), the circulation
85 showed a weakening of the stratospheric polar vortex. However, a strengthened polar vortex
86 was found with prescribed sea ice loss outside the Arctic Circle, largely over the Pacific
87 ocean.

88 In this study, we investigate the response of NH midlatitude circulation to AA in an
89 idealized dry AGCM. In particular, we aim to address two key questions:

- 90 i. What is the robust response in the troposphere and stratosphere to AA?
- 91 ii. What is the role of stratosphere-troposphere coupling in driving the midlatitude cir-
92 culation response to AA?

93 The idealized dry AGCM largely isolates the dynamics from uncertainties arising from com-
94 plex physical parameterizations and a thorough but computationally affordable exploration
95 of parameter sensitivities can be performed. More importantly, the idealized model allows
96 for an explicit separation of tropospheric and stratospheric pathway, which may not be easily
97 accomplished in comprehensive AGCMs.

98 This paper is organized as follows. In Section 2 we describe the model setup, numerical
99 experiments and diagnostic methods used in this study. In Section 3 we analyze the response

100 in the troposphere and stratosphere to AA and the role of stratosphere-troposphere coupling.
101 A discussion in Section 4 concludes the paper.

102 **2. Model Experiments and Methods**

103 *a. Model Setup*

104 We use a simplified AGCM as described in Smith et al. (2010) (hereafter SFK10). The
105 model is a dry dynamical core, developed by the Geophysical Fluid Dynamics Laboratory,
106 that integrates the primitive equations driven by idealized physics (Held and Suarez 1994).
107 The temperature field is linearly relaxed to an analytical radiative equilibrium temperature
108 profile, T_{eq} , that is zonally symmetric. For a simple representation of stratospheric condi-
109 tions, the relaxation temperature is modified to include a polar vortex, the strength of which
110 is determined by a temperature lapse rate, γ (Polvani and Kushner 2002). Following Smith
111 et al. (2010), the model configuration used here consists of $\gamma = 2$ K/km and $\epsilon = 10$ for
112 NH perpetual winter conditions. The model also uses realistic topography which allows for
113 the excitation of a rather realistic planetary-scale stationary wave pattern. We integrate the
114 model for 20,000 days at T42 horizontal resolution with 40 levels in the vertical and a model
115 lid at 0.02 hPa.

116 The primary reason we choose the SFK10 model version for our study is that this model
117 has a reasonable representation of the stratosphere and its variability. As to be demonstrated
118 in Section 3, the maximal strength of polar vortex at 10 hPa is about 30 m/s, and the
119 frequency of sudden stratospheric warmings (SSW) is about 0.27 per 100 days (smaller than
120 observed, to be discussed later). More importantly, this model version has a tropospheric
121 jet located near 40°N, which is close to observed circulation in NH winter.

122 Despite simulating the opposite signed response compared to observations and compre-
123 hensive GCM simulations, Smith et al. (2010) successfully used this model to understand
124 the dynamical mechanisms underlying the wintertime NAM driven by autumn snow cover

125 anomalies over Siberia. They found that the model was able to successfully capture the
 126 troposphere-stratosphere coupling. The anomalous autumn snow cover and resulting re-
 127 gional surface cooling generates planetary-scale wave anomaly that is in phase with the cli-
 128 matology, and as a result of constructive interference, the upward propgating wave anomaly
 129 into the stratosphere is further amplified, leading to a weakening of stratospheric polar vor-
 130 tex. This NAM anomaly migrates downward into the troposphere and affects the surface
 131 weather in the subsequent winter (Fletcher et al. 2009).

132 *b. Numerical Experiments*

133 To isolate the effect of AA, we follow the methodology of Butler et al. (2010) and add a
 134 simple AA-like thermal forcing, maximized at the northern polar surface, to the temperature
 135 equation:

$$136 \quad \frac{\partial T}{\partial t} = \dots - \kappa_T(\phi, \sigma)[T - (T_{eq}(\phi, \sigma) + T_{eq}^{AA}(\phi, \sigma))] \quad (1)$$

137 where κ_T is the Newtonian relaxation time and T_{eq} , as a function of latitude ϕ and sigma
 138 level σ , is the original radiative equilibrium temperature profile in Smith et al. (2010) that
 139 includes a stratospheric polar vortex. The perturbation, T_{eq}^{AA} , is designed to mimic AA and
 140 can be written as:

$$141 \quad T_{eq}^{AA}(\phi, \sigma) = \begin{cases} T_0^{AA} \cos^k(\phi - 90^\circ) e^{m(\sigma-1)} & \text{for } \phi > 0 \\ 0 & \text{for } \phi \leq 0 \end{cases} \quad (2)$$

142 where T_0^{AA} is the perturbation magnitude, and k and m are parameters that determine the
 143 latitudinal and vertical extent of the warming perturbation, respectively. This analytical
 144 formula of T_{eq}^{AA} is adopted from Butler et al. (2010), where they examined the scenario where
 145 $k = 15$, $m = 6$ and a maximum heating rate of 0.5 K/day (which is approximately equivalent
 146 to $T_0^{AA} = 20$ K assuming a relaxation time scale of 40 days) and found an equatorward shift
 147 of the tropospheric jet.

148 Here we derive T_{eq}^{AA} from the projected zonal mean temperature response during 2080-
 149 2099 in the Representative Concentration Pathway (RCP) 8.5 scenario, compared to 1980-
 150 1999 in the historical scenario, averaged across 30 models participating in the Coupled
 151 Model Intercomparison Projection phase 5 (CMIP5) project. Figure 1 shows the zonal mean
 152 temperature response averaged over November-December, the season of maximum AA in
 153 CMIP5 multi-model averages. It comprises a large tropical upper tropospheric warming and
 154 an even larger NH AA as well as stratospheric cooling. It is worth noticing that the projected
 155 AA not only concentrates near the surface but also extends to the mid-troposphere. We fit
 156 the CMIP5 temperature response with the T_{eq}^{AA} in Equation (2) with $T_0^{AA} = 15$ K, $k = 5$, and
 157 $m = 3$. To investigate the sensitivity of the circulation response to the forcing, we vary T_0^{AA}
 158 over a range of forcing strengths, i.e. $T_0^{AA} = 5, 10, 15, 20, 25$ K, while fixing the meridional
 159 and vertical extent of the forcing, i.e. $k = 5$, and $m = 3$. The control experiment in the
 160 absence of AA is denoted by CTRL and the sensitivity experiments forced with imposed AA-
 161 like forcings are denoted by AA5, AA10, AA15, AA20 and AA25, respectively, for various
 162 forcing magnitudes.

163 We emphasize here that our study of AA is different from some previous studies in that
 164 it is not limited to the effect of Arctic sea ice loss. Instead we focus on the rather deep
 165 and wide warming at northern high latitudes, and as shown in Fig. 1, the 5 K warming
 166 extends to about 50°N and 600 hPa. As discussed previously, this feature of AA is likely
 167 due to many factors such as longwave radiation feedback, lapse rate feedback, increased
 168 moisture transport and increased oceanic transport (references in Collins et al. 2013; Pithan
 169 and Mauritsen 2014).

170 In addition, in order to separate the tropospheric and stratospheric pathway, we make
 171 use of a nudging method as in Simpson et al. (2011, 2013). To isolate the tropospheric
 172 circulation response to AA via the tropospheric pathway only, the zonal mean (wave 0)
 173 vorticity, divergence, and temperature in the stratosphere are nudged towards the reference
 174 state in the CTRL experiment. This is done via a simple relaxation in spectral space at every

175 time step: $-K(\sigma)(X - X_0)/t_N$, where X is the instantaneous value of a given field (vorticity,
 176 divergence or temperature), X_0 is the reference state, t_N is the nudging time scale (we
 177 choose a nudging time scale of six times the integration time step), and $K(\sigma)$ is the nudging
 178 coefficient that is 1 above 28 hPa, 0 below 64 hPa and linear interpolation in between. The
 179 essence of the nudging method is that it shuts down the stratosphere-troposphere coupling
 180 by fixing the stratospheric zonal mean state at every time step. We construct a NUDG AA
 181 experiment where we impose AA-like forcing near the surface while nudging the stratospheric
 182 zonal mean state to that of the CTRL experiment. Then in the NUDG AA experiment,
 183 the response in the midlatitude troposphere is purely via the tropospheric pathway and is
 184 accomplished by tropospheric waves and wave-mean flow interaction. If we assume that the
 185 circulation response via the tropospheric and stratospheric pathways is linearly additive, then
 186 the stratospheric contribution to the total response can be obtained by the difference of the
 187 total response and response via the tropospheric pathway only in the nudging experiment.
 188 In order to confirm the stratospheric pathway, we also perform a NUDG downward-AA
 189 experiment by nudging the stratospheric zonal mean state to that of the AA experiment and
 190 imposing no thermal forcing near the surface.

191 Finally, we make use of a zonally symmetric version of the SFK10 model. Following
 192 Kushner and Polvani (2004), we first construct the eddy forcing, at each time step, as the
 193 negative tendency of the zonal and time mean state of the primitive equation model, and
 194 then use the computed eddy forcing to drive the zonally symmetric model. The zonally
 195 symmetric configuration has been widely used and is useful to further separate the direct
 196 thermally forced response and the effect of eddy feedbacks, specifically in the troposphere
 197 and in the stratosphere, respectively. As in Kushner and Polvani (2004), we perform a ZSYM
 198 E^{strat} experiment with the eddy forcing confined in the stratosphere by applying a smooth
 199 weighting function to the eddy forcing.

200 In summary, Table 1 lists all the experiments performed in this study.

201 *c. Diagnostics*

202 We estimate the magnitude of AA as the Arctic (67.5°N to 90°N) near-surface tempera-
 203 ture increase in T_{eq}^{AA} . In AA5, AA10, AA15, AA20, and AA25 experiments, the AA is about
 204 3.49, 6.97, 10.46, 13.94, 17.43 K, respectively. As described above, the AA15 experiment is
 205 close to the RCP8.5 scenario at the end of the 21st century. As in Table 12.2 of Collins et al.
 206 (2013), the projected annual mean Arctic temperature increase is about 8.3 ± 1.9 K across
 207 CMIP5 models, and our imposed AA-forcing strength in AA15 is slightly larger because of
 208 the focus on winter season.

209 Second, to diagnose wave-mean flow interaction, we use the Eliassen-Palm (EP) flux
 210 in spherical and pressure coordinates, $\vec{F} = [F_{(\phi)}, F_{(p)}]$, and it is calculated as $F_{(\phi)} =$
 211 $-a \cos \phi \langle u^* v^* \rangle$ and $F_{(p)} = af \cos \phi \frac{\langle v^* \theta^* \rangle}{\langle \theta \rangle_p}$, where f is the Coriolis parameter, θ is potential
 212 temperature, bracket denotes zonal average and asterisk denotes deviation from zonal aver-
 213 age (Edmon et al. 1980). The direction of the flux vectors generally indicates the propagation
 214 of waves and the flux divergence, calculated as $\frac{1}{a \cos \phi} \nabla \cdot \vec{F} = \frac{1}{a \cos \phi} \left\{ \frac{1}{a \cos \phi} \frac{\partial}{\partial \phi} (F_{(\phi)} \cos \phi) + \right.$
 215 $\left. \frac{\partial}{\partial p} F_{(p)} \right\}$, measures the wave forcing on the zonal mean flow.

216 Third, we make use of two methods to identify sudden stratospheric warming (SSW)
 217 events, which are dramatic dynamical events in the NH and are characterized by a rapid
 218 increase of polar cap temperature and a reversal of westerly wind. The first is a standard
 219 method, which identifies a SSW when the daily zonal mean zonal wind at 10 hPa, cosine-
 220 weighted and averaged over 60-90°N, drops below zero, with at least 45 days between two
 221 SSW events (e.g., Charlton and Polvani 2007; Butler et al. 2015). The second is the NAM
 222 method. The NAM at each pressure level is defined as the 1st EOF of daily zonal mean
 223 zonal wind anomalies poleward 20°N, weighted by square root of the cosine of latitude, and
 224 then the NAM index is generated by projecting the unweighted original anomalies onto the
 225 1st EOF, further standardized to unit variance. So the positive phase of the NAM, at 10
 226 hPa for example, is associated with positive zonal wind poleward of about 45°N. A SSW

227 event is defined to occur when the 10 hPa NAM index drops below -2.0 standard deviations
228 and again with at least 45 days between two SSW events (e.g., Gerber and Polvani 2009).
229 By using these two methods, we aim to provide a robust assessment of the SSW response to
230 imposed AA.

231 Lastly, a couple of technical notes. Almost all the numerical experiments are integrated
232 for 20,000 days with the first 1,000 days of spin up discarded, and the zonally symmetric
233 model experiments are run for 2,000 days. For most climate variables, time averages are
234 taken during the first 9,000 days (averages over 9,000 days are sufficient and similar results
235 are obtained with the last 10,000 days of integrations) except for SSW for which 19,000 days
236 are included. For all variables, statistical significance is evaluated via a simple Student's t
237 test, using the 95% confidence interval. For the calculation of SSW frequency, the confidence
238 interval is constructed by using the bootstrap method, which independently resamples the
239 results with replacement for 1,000 times. The confidence interval is then calculated as the
240 2.5th and 97.5th percentiles from resamplings.

241 **3. Results**

242 *a. Circulation Response in Troposphere and Stratosphere*

243 First, Fig. 2(a) shows the climatological zonal mean zonal wind in the SFK10 model. The
244 simulated circulation mimics the NH perpetual winter conditions which are characterized by
245 a strong NH stratospheric polar vortex and a midlatitude jet located near 40°N in the lower
246 troposphere.

247 As a result of imposed AA-like forcings, for various forcing strengths, the circulation
248 response robustly exhibits an equatorward shift of the NH tropospheric jet, with a weakening
249 of the zonal wind on the poleward flank and a strengthening on the equatorward flank. This
250 is perhaps not surprising and is in agreement with many previous studies (e.g., Deser et al.
251 2004; Peings and Magnusdottir 2014). More importantly, there is a robust weakening of the

252 stratospheric polar vortex, which was also identified in some previous studies (e.g., Peings
253 and Magnusdottir 2014; Feldstein and Lee 2014; Kim et al. 2014). The weakening of the
254 stratospheric polar vortex appears to be coupled with the equatorward displaced tropospheric
255 jet, which resembles the negative phase of NAM. In our model configuration, there appears
256 to be no response in the Southern Hemisphere. When the AA-like forcing is weak, as in
257 Fig. 2(b), the tropospheric jet response is also rather weak and the stratospheric response is
258 confined to the lower stratosphere. As the forcing becomes larger, the circulation response
259 also becomes stronger (Fig. 2(f)).

260 To better quantify the zonal mean zonal wind response, Fig. 3 shows the position and
261 strength of maximal wind at 841, 256, and 10 hPa. The zonal mean zonal wind is first inter-
262 polated onto a 0.1° grid using a cubic spline interpolation before calculating the jet latitude
263 and intensity. In the lower troposphere, in response to AA-like forcings, the jet position
264 moves equatorward and the maximal wind speed decelerates. In the upper troposphere, the
265 jet also shifts equatorward but the maximal wind speeds up slightly. It is noted that the
266 thermal wind balance approximately holds here, where the decrease in meridional temper-
267 ature gradient is in balance with the decrease of zonal wind with altitude (not shown). In
268 the stratosphere there is a general poleward displacement and weakening of the polar vor-
269 tex. In the AA15 experiment, which is similar to the projected AA in the RCP8.5 scenario,
270 the lower-tropospheric jet shifts equatorward by about 4° latitude and weakens by about
271 0.5 m/s, the upper-tropospheric jet shifts equatorward by 4° latitude and strengthens by
272 0.5 m/s, and the stratospheric jet moves poleward by 2° latitude and weakens by 5 m/s.
273 Although in general, the larger the forcing, the larger the response, there also appears to be
274 a tendency for the response to saturate.

275 To better interpret the weakening of the stratospheric polar vortex, Fig. 4(a)(b) shows
276 the EP flux and its divergence in the control and AA15 experiment, as an example. The
277 climatological flux vectors clearly indicate that the waves are generated in the lower tropo-
278 sphere, presumably as a result of baroclinic instability and orographic forcing, and propagate

279 upward and equatorward. The response to imposed AA forcing shows more upward propa-
 280 gating waves poleward of about 62°N as well as wave anomalies propagating northward in
 281 the stratosphere poleward of 62°N above 100 hPa. It is largely the northward flux anomaly
 282 and its convergence of momentum flux that contributes to an increase of net EP flux con-
 283 vergence (i.e., $\nabla \cdot \vec{F} < 0$) in the stratosphere and a weakening of the polar vortex. In the
 284 midlatitude troposphere, the response in EP flux is almost opposite in sign to that of the
 285 climatology and is associated with the equatorward tropospheric jet shift. This EP flux
 286 response is qualitatively similar in other forcing strength experiments (not shown).

287 Furthermore, to better understand the response in wave activity in our idealized exper-
 288 iments, we follow the method in Smith et al. (2010) and decompose the response in eddy
 289 meridional heat flux into time-mean (TM) linear, time-mean nonlinear, and fluctuation com-
 290 ponents:

$$\begin{aligned}
 291 \quad \Delta \langle \overline{v^* T^*} \rangle &= \text{TM}_{\text{LIN}} + \text{TM}_{\text{NONLIN}} + \text{FL} \\
 292 \quad \text{TM}_{\text{LIN}} &= \langle (\Delta \bar{v}^*) \bar{T}_c^* \rangle + \langle (\Delta \bar{T}^*) \bar{v}_c^* \rangle \\
 293 \quad \text{TM}_{\text{NONLIN}} &= \langle \Delta \bar{T}^* \Delta \bar{v}^* \rangle \\
 294 \quad \text{FL} &= \Delta \langle \overline{v'^* T'^*} \rangle
 \end{aligned}$$

295 where v and T are daily variables, Δ is the difference between AA and control experiment,
 296 subscript c denotes the control experiment, bar denotes time average, prime denotes deviation
 297 from time average, $\langle \rangle$ denotes zonal average, and superscript $*$ denotes deviation from zonal
 298 average. In the prescribed Siberian snow forcing experiments of Smith et al. (2010) with the
 299 same model setup, linear interference was found to work well to explain the response in wave
 300 activity, which was dominated by the TM_{LIN} component, and wave activity was amplified
 301 in constructive interference when the wave anomaly was in phase with the climatology. The
 302 FL term, which is associated with high-frequency wave components, and $\text{TM}_{\text{NONLIN}}$ were
 303 found to be small.

304 However, the heat flux decomposition seems more complicated in our imposed AA forc-

305 ing experiments and linear interference is not the dominant mechanism at high latitudes.
306 Figure 4(c)-(f) shows the response in zonal mean eddy heat flux and its decomposition. The
307 response in meridional heat flux shows an increase at high latitudes and a decrease in mid-
308 latitudes, which is in agreement with the response in EP flux (Fig. 4(b)). Although our
309 AA forcing is zonally symmetric, the interaction between the AA forcing and the zonally
310 asymmetric lower boundary condition excites planetary-scale Rossby waves at high latitudes
311 (primarily wave-1, not shown). The increased heat flux at high latitudes is mostly due to
312 the nonlinear component, and to a lesser extent, the high frequency wave contribution. The
313 linear component seems to contribute to the increased heat flux in the troposphere high
314 latitudes but certainly not in the stratosphere high latitudes.

315 This seems to be different from some previous studies that found increased upward wave
316 propagation as a result of the sea ice loss over the B-K sea and attributed the mechanism
317 to wave constructive interference (e.g., Peings and Magnusdottir 2014; Feldstein and Lee
318 2014; Kim et al. 2014; Sun et al. 2015). Although we do not have a full explanation yet,
319 the model setup and imposed forcing are completely different in our study. The model
320 is a dry primitive equation model and may have some deficiencies in fully capturing the
321 circulation at high latitudes. More importantly, we impose a zonally symmetric forcing
322 whereas previous studies all focused on regional sea ice loss and associated surface flux
323 and temperature increase. A study by Garfinkel et al. (2010) examined the tropospheric
324 precursors to stratospheric polar vortex weakening and found the North Pacific low and
325 the eastern European high most effective in modulating the polar vortex. A low anomaly
326 of geopotential height, for example, during the October snow anomaly over Eurasia, could
327 constructively interfere with the climatological northwestern Pacific low and amplify the
328 wave activity into the stratosphere, resulting in a weakening of the polar vortex, as seen in
329 Cohen et al. (2007) and Smith et al. (2010). The sea ice loss over the B-K sea and resulting
330 high anomaly of geopotential height happens to be collocated with the eastern European
331 high and could effectively increase the upward wave propagation into the stratosphere (e.g.,

332 Kim et al. 2014). However, this is not the same in our study. A zonally symmetric forcing
333 over the entire Arctic could excite more complicated waves and the mechanism of linear
334 interference might no longer play a dominant role.

335 Figure 5 shows the zonal wind response at 513 hPa. In the control experiment, the zonal
336 wind peaks over the North America North Atlantic sector and the Asia-North Pacific sector.
337 The equatorward displacement of zonal wind, as a result of AA, is found to maximize over
338 the North Atlantic and North Pacific sectors, which projects onto the climatological zonal
339 wind pattern. The zonal wind response is generally robust across various forcing strengths.

340 Finally, since the time mean stratospheric polar vortex weakens as a result of AA, next
341 we assess whether there is a change in stratospheric variability, in particular, SSW frequency
342 (e.g., Jaiser et al. 2013). First of all, in the control experiment, the SSW frequency is about
343 0.27 per 100 days as defined by the standard method with a reversal of zonal mean westerly
344 wind at 10hPa poleward of 60°N (as shown in Fig. 6(a)). A similar result is found using the
345 NAM method (0.25 per 100 days, shown in Fig. 6(b)). The SFK10 model under-estimates
346 the observed SSW frequency (e.g., Butler et al. (2015) estimated 0.91 per winter season from
347 November to March, or equivalently about 0.61 per 100 days, using the ERA reanalyses and
348 similar reversal of westerly wind method); however, this behavior is found to be rather
349 common even among state-of-the-art climate models (e.g., Charlton-Perez and Coauthors
350 2013). Figure 6 shows the SSW response and its confidence interval as a consequence of the
351 imposed AA forcing. In general, both the standard and NAM methods¹ show no statistically
352 significant change in the SSW frequency. The SSW response using the standard method is
353 rather minor, except for the AA5 experiment, where a decrease compared to control is seen
354 at marginal significance level. The response in the NAM method seems to show a small
355 rising trend as AA strength increases, but not statistically significant, perhaps except for

¹For the calculation of the NAM index in various AA forcing strength experiments, we have also tried projecting the anomalies onto the 1st EOF from the CTRL experiment and have obtained nearly identical results.

356 a marginally significant increase in the largest AA forcing experiment. We note here that
357 the precise choice of the parameters in SSW definitions (such as the latitude and recovery
358 period) has no effect on the conclusions drawn in this paper.

359 To aid the interpretation of the modeled SSW response to AA, Fig. 7 shows the time
360 mean meridional eddy heat flux $\langle v^*T^* \rangle$ at 100 hPa. It can be seen in Fig. 7(a) that, at
361 mid-to-high latitudes, poleward of 45°N , the response in meridional heat flux exhibits a
362 dipole structure, with an increase northward of 60°N and a decrease equatorward. The
363 increase of meridional heat flux at high latitudes is likely due to the near-surface AA and
364 resulting increased upward planetary-scale wave propagation. The equatorward shift of the
365 tropospheric jet is associated with an equatorward shift of the baroclinic instability zone and
366 therefore the meridional heat flux, leading to a decrease of $\langle v^*T^* \rangle$ over $45\text{-}60^\circ\text{N}$. Figure 7(b)
367 shows the average of $\langle v^*T^* \rangle$ poleward of 45°N , weighted by the cosine of latitude, and the
368 change is rather small compared to the control experiment, i.e. only about 2% for most of
369 the forcing strengths. This is due to the cancellation between the increase at high latitudes
370 and decrease at midlatitudes. Therefore, in summary, we find that there is no significant
371 change in net meridional heat flux at mid-to-high latitudes and this seems to be in agreement
372 with no significant change in SSW frequency as a result of AA.

373 *b. The Role of Troposphere and Stratosphere Pathway*

374 The equilibrium circulation response, as seen in Fig. 2, likely consists of the response
375 via both tropospheric and stratospheric pathway. The tropospheric circulation response via
376 the tropospheric pathway is associated with the adjustment of transient eddies, due to the
377 change in meridional temperature gradient and baroclinic instability. On the other hand,
378 the stratospheric pathway involves enhanced upward planetary-scale wave propagation and
379 the weakening of the stratospheric polar vortex as a result of AA that could modify the
380 tropospheric circulation response. In order to distinguish the two pathways, we "deactivate"
381 the stratospheric pathway by nudging the stratospheric zonal mean state towards a reference

382 state in the CTRL experiment (details described in Section 2). As described above, although
383 waves can propagate freely into the stratosphere, they almost have no influence on the
384 stratospheric zonal mean state because of the nudging and therefore, there is no zonal mean
385 anomaly that could propagate downward back to the troposphere.

386 Before discussing the key results, we first demonstrate that the nudging method is indeed
387 acting to largely damp the zonal mean stratospheric variability. Figure 8 shows the amplitude
388 of the NAM pattern of variability in the CTRL and NUDG experiments. Following Gerber
389 and Coauthors (2010) and Simpson et al. (2013), we first compute the NAM and NAM index
390 (as above in the calculation of SSW). We then construct the NAM pattern by regressing
391 the daily zonal mean zonal wind anomalies onto the NAM index, and compute the NAM
392 amplitude as the root-mean-square of the NAM pattern weighted by the cosine of latitude. In
393 Fig. 8, the CTRL experiment shows a tropospheric NAM pattern of variability, maximized
394 in the mid-to-upper troposphere, and a larger stratospheric variability which increases with
395 height. We also show the same diagnostic for the nudging experiments and it is clear that,
396 in all the nudging experiments, the stratospheric variability is largely reduced while the
397 tropospheric variability is essentially unaffected.

398 Next we choose AA15 as a primary example to demonstrate the tropospheric and strato-
399 spheric pathway, and other forcing strengths are qualitatively similar. Figure 9(a)(b)(c)
400 shows the zonal mean zonal wind in the CTRL and AA15 experiment and their difference,
401 respectively, which is the same as Fig. 2(d). Figure 9(d) shows the zonal mean zonal wind
402 in the nudging experiment and Fig. 9(e) shows the response, which is obtained via the
403 tropospheric pathway only. As shown in Fig. 9(e), the stratospheric zonal mean state is
404 largely unaffected and the tropospheric circulation exhibits an equatorward displacement
405 with a decrease in zonal wind on the poleward flank and an increase on the equatorward
406 flank, which is similar in pattern but smaller in magnitude than the total response seen in
407 Fig. 9(c). Results are found to robust with the last 10,000 days of integrations (not shown).
408 We also note here that we perform an additional NUDG CTRL experiment, in which we

409 nudge the stratospheric zonal mean state towards that of the CTRL. We find that the zonal
410 mean zonal wind in both the troposphere and stratosphere in the NUDG CTRL experiment
411 is almost identical to that of the CTRL experiment (not shown).

412 If we assume that the circulation response via the tropospheric pathway and strato-
413 spheric pathway are linearly additive, the difference between the total response and the
414 response via the tropospheric pathway can be interpreted as the response via the strato-
415 spheric pathway and stratosphere-troposphere coupling (shown in Fig. 9(f)). The response
416 via the stratospheric pathway shows a weakening of the stratospheric polar vortex as well as
417 an equatorward shift of the tropospheric jet, which resembles the downward influence from
418 the stratosphere on the troposphere as found in many previous studies such as Baldwin and
419 Dunkerton (2001). This effect on the tropospheric circulation is certainly non-negligible and
420 is, in fact, similar in magnitude to that via the tropospheric pathway only. This suggests
421 that the stratospheric pathway and stratosphere-troposphere coupling plays a significant role
422 in determining the midlatitude tropospheric circulation response to AA.

423 Next we confirm that the circulation response, as seen in Fig. 9(f), is indeed the downward
424 influence from the stratosphere on the troposphere. To do that, we nudge the stratospheric
425 zonal mean state to that of the AA15 experiment (as in Fig. 9(b)) with no prescribed ther-
426 mal forcing near the surface. Figure 10(a) shows the circulation response in this NUDG
427 downward-AA15 experiment. The response is almost identical to Fig. 9(f). In particular,
428 the equatorward shift of the tropospheric jet is indistinguishable from that of Fig. 9(f), con-
429 firming that this is indeed the downward influence of the stratosphere on the troposphere. In
430 addition, we note here that the circulation response via the stratospheric pathway is accom-
431 plished not only by stratospheric wave-mean flow interaction, but also by the tropospheric
432 eddy feedback. To briefly demonstrate this, we examine the circulation response in the zon-
433 ally symmetric model configuration. First, we confirm that when the eddy forcing is applied
434 the zonally symmetric model is able to reproduce the total response in the full model as seen
435 in Fig. 9(c) (not shown). Then, we investigate the importance of downward control to the

436 tropospheric response by confining the eddy forcing to the stratosphere only (Haynes et al.
437 1991; Kushner and Polvani 2004). By eliminating the tropospheric eddy feedback, Figure
438 10(b) shows that, although the stratospheric wind response is able to penetrate into the tro-
439 posphere, there is no clear equatorward shift of the jet and no coupling to the surface. This
440 is in agreement with previous studies such as Kushner and Polvani (2004) and Domeisen
441 et al. (2013). Thus we conclude that the circulation response is indeed the downward influ-
442 ence from the stratosphere on the troposphere and requires tropospheric eddy feedback in
443 addition to stratospheric eddy forcing.

444 Finally, in order to quantitatively measure the role of an active stratosphere, we calculate
445 the jet position and intensity as in Fig. 3 but now including the results of the NUDG AA
446 experiments (shown in Fig. 11). Again the jet position and intensity in the stratosphere
447 in the nudging experiments, by design, is largely unaffected (Fig. 11(e)(f)). However, in
448 both the lower and upper troposphere, consistently for various forcing strengths, the re-
449 sponse via the tropospheric pathway is almost always about half of the total response and
450 the other half is accomplished via the stratospheric pathway. Therefore, in summary, by
451 using the nudging method, we are able to explicitly separate the tropospheric and strato-
452 spheric pathway. We find that, in response to AA, coupling between the stratosphere and
453 the troposphere *significantly* enhances the midlatitude tropospheric circulation response by
454 shifting the tropospheric jet further equatorward.

455 A final note before the conclusions - the effect of the stratospheric pathway is found
456 to be robust in a slightly different model configuration. In addition to SFK10, we also
457 perform a similar set of AA and NUDG AA experiments using the Gerber and Polvani
458 (2009) configuration (hereafter GP09) with an idealized wave-2 topography. With the GP09
459 model version and some modifications to simulate a tropospheric jet with a more realistic
460 location (near 42°N), we find qualitatively similar results and the stratospheric pathway also
461 significantly shifts the tropospheric jet equatorward. Details of the model setup and results
462 are provided in Appendix and Fig. 12.

4. Discussion and Conclusions

We have examined the NH midlatitude circulation response to imposed AA-like thermal forcing in a simple AGCM. In particular, we have focused on two key aspects - first, on the robust circulation response in the troposphere and stratosphere, and second, on the role of stratosphere-troposphere coupling in determining the midlatitude circulation. For the first part, we have found that, as a result of AA, the tropospheric jet shifts equatorward and the stratospheric polar vortex weakens, which is robust for various forcing strengths. We have also calculated the frequency of SSWs and found no statistically significant change in SSWs, which is in agreement with no significant change in meridional heat flux.

For the second part, we have explicitly separated the tropospheric and stratospheric pathway by nudging the stratospheric zonal mean state in the AA experiments to the reference state in the control. We have found that, by shutting down the stratosphere-troposphere coupling, the tropospheric circulation still shifts equatorward but to a lesser extent (about half the magnitude). As for the tropospheric pathway and its underlying mechanism, it was discussed extensively in Deser et al. (2004) and others and is beyond the scope of this study. The difference between the total and nudged response, which we argue represents the stratospheric pathway, i.e., the downward influence of the stratosphere on the troposphere, also shows an equatorward shift of the tropospheric jet, similar in magnitude to that of the tropospheric pathway. Therefore, this suggests that an active stratosphere and its coupling with the troposphere plays a significant role in determining the tropospheric circulation response to AA.

In this study, we have demonstrated, for the first time, that the stratospheric pathway could be potentially as important as the tropospheric pathway. Although Sun et al. (2015) found a stronger circulation response to Arctic sea ice loss in high-top WACCM4 compared to low-top CAM4 and suggested a stratospheric pathway, the two models have different climatological mean states and stratospheric variability and the underlying mechanisms are potentially complex. Here, we have presented a cleaner separation of the tropospheric and

490 stratospheric pathways using a single model and we are able to quantitatively estimate the
491 relative importance of the two pathways.

492 One possible caveat of this study is the use of zonally symmetric AA forcing. In future
493 climate projections, the Arctic sea ice loss and AA are not zonally symmetric (e.g., Figs.
494 12.11 and 12.29 of Collins et al. 2013). In fact, as demonstrated in Sun et al. (2015), at the
495 end of the century, most of the sea ice loss within the Arctic Circle is projected to occur in
496 the B-K Sea and the Pacific outside the Arctic Circle. The effects from sea ice loss in these
497 two sectors, however, tend to drive opposite responses in upward wave propagation and the
498 stratospheric polar vortex. In future study, we plan to consider zonally asymmetric forcings
499 in different regions. Secondly, this study is focused solely on the effect of AA in an idealized
500 dry model and the implication for future climate change needs to take many other factors
501 into account such as the extensive warming in the tropical upper troposphere. Barnes and
502 Polvani (2015) examined the projected changes in North American/North Atlantic circula-
503 tion in CMIP5 models and found that AA might modulate some aspects of the circulation
504 response but is unlikely to dominate. Finally, our study investigates the equilibrium circula-
505 tion response in perpetual winter conditions and doesn't consider the possible delaying effect
506 from the stratosphere. Sun et al. (2015) imposed sea ice loss only in autumn and found a
507 significant tropospheric circulation response in late winter and early spring, possibly through
508 the stratospheric pathway. We plan to further investigate the role of stratospheric pathway
509 in transient simulations in the future.

510 In this study, we have demonstrated that stratosphere-troposphere coupling plays a non-
511 negligible role in setting up the tropospheric circulation response to high latitude near-surface
512 warming. Our results provide further evidence that use of stratosphere-resolving GCMs is
513 critical in order to fully simulate the circulation response to climate change (e.g., Charlton-
514 Perez and Coauthors 2013).

515 5. Appendix

516 As described in Section 2, we choose the SFK10 model because of the representation of
517 the stratospheric circulation and its variability as well as the tropospheric jet position. Here
518 we demonstrate the robustness of the results by using a slightly different model configuration
519 that has also been widely used in the community.

520 We make use of the Gerber and Polvani (2009) model version (hereafter GP09), in which
521 $\gamma = 4$ K/km and an idealized wave-2 topography is imposed. As demonstrated in Gerber
522 and Polvani (2009), the combination of $\gamma = 4$ K/km and wave-2 topography has the most
523 realistic stratosphere-troposphere coupling. While the GP09 model generates planetary-scale
524 stationary waves and produces rather realistic stratospheric variability, the low-level jet is
525 located near 30°N , which is a bit too equatorward compared to the observed wintertime
526 jet position. In order to move the tropospheric jet northward to mimic the observed winter
527 conditions, we follow Garfinkel et al. (2013) and add two additional terms to the T_{eq} equation,
528 as in Eq. (2) of Garfinkel et al. (2013). By setting $A = 5$ and $B = 2$, we are able to shift the
529 tropospheric jet to about 42°N . Figure 12(a) shows the zonal mean zonal wind and it has a
530 tropospheric jet located at 42°N and a stronger stratospheric polar vortex than the SFK10
531 version.

532 However, we find that the frequency of SSWs is reduced by a large amount as the tro-
533 pospheric jet moves poleward. With a jet near 30°N , the SSW frequency is about 0.3 per
534 100 days; however, with a jet near 42°N , the SSW frequency decreases to 0.08 per 100 days.
535 This issue of SSW shut down has also been identified in Wang et al. (2012) (not shown) and
536 is probably due to the regime behavior in model setup (E. Gerber 2015, personal communi-
537 cation). This issue could be a major concern in the discussion of stratosphere-troposphere
538 coupling as SSWs are important dynamical events that have the potential to migrate down-
539 ward and affect near-surface weather pattern (e.g., Baldwin and Dunkerton 2001; Polvani
540 and Waugh 2004).

541 Nonetheless, we examine the midlatitude circulation response to imposed AA forcings in

542 this model version, in particular, the role of stratosphere-troposphere coupling. In response
543 to AA15, as an example, the stratospheric polar vortex shows a general weakening (with some
544 strengthening at high latitudes), and the tropospheric jet moves equatorward (shown in Fig.
545 12(c)). With the same nudging method applied in the stratosphere as NUDG AA, Fig. 12(e)
546 shows the circulation response via the tropospheric pathway and has the tropospheric jet
547 shifted equatorward as well, but to a lesser extent. Figure 12(f) shows the response via
548 stratosphere-troposphere coupling and it resembles the downward influence from the strato-
549 sphere on the troposphere. The zonal mean zonal wind response is similar in the midlatitude
550 troposphere between the tropospheric pathway (Fig. 12(e)) and stratospheric pathway (Fig.
551 12(f)). This demonstrates that an active stratosphere indeed acts to significantly intensify
552 the tropospheric circulation response to AA and this is in agreement with the SFK10 model
553 configuration.

554 *Acknowledgments.*

555 The authors would like to thank Lorenzo M. Polvani and Clara Deser for helpful discus-
556 sions. The authors acknowledge the World Climate Research Programme's Working Group
557 on Coupled Modelling, which is responsible for CMIP, and we thank the climate modeling
558 groups for producing and making available their model output. For CMIP the U.S. De-
559 partment of Energy's Program for Climate Model Diagnosis and Intercomparison provides
560 coordinating support and led development of software infrastructure in partnership with the
561 Global Organization for Earth System Science Portals. YW is supported, in part, by the
562 US National Science Foundation (NSF) Climate and Large-Scale Dynamics program under
563 Grant AGS-1406962. KLS is funded by a Natural Sciences and Engineering Research Council
564 of Canada (NSERC) Postdoctoral Fellowship.

REFERENCES

- 567 Baldwin, M. P. and T. J. Dunkerton, 2001: Stratospheric harbingers of anomalous weather
568 regimes. *Science*, **294**, 581–584.
- 569 Barnes, E. and L. Polvani, 2015: CMIP5 projections of Arctic amplification, of the North
570 American/North Atlantic circulation, and of their relationship. *J. Clim.*, **28**, 5254–5271.
- 571 Barnes, E. A. and J. Screen, 2015: The impact of Arctic warming on the midlatitude jet-
572 stream: Can it? Has it? Will it? *WIREs Climate Change*, **6**, doi: 10.1002/wcc.337.
- 573 Butler, A., D. Seidel, S. Hardiman, N. Butchart, T. Birner, and A. Match, 2015: Defin-
574 ing sudden stratospheric warmings. *Bull. Amer. Meteor. Soc.*, doi:10.1175/BAMS-D-13-
575 00173.1, in press.
- 576 Butler, A. H., D. W. J. Thompson, and R. Heikes, 2010: The steady-state atmospheric
577 circulation response to climate change-like thermal forcings in a simple general circulation
578 model. *J. Clim.*, **23**, 3474–3496.
- 579 Cai, D., M. Dameris, H. Garny, and T. Runde, 2012: Implications of all season Arctic sea-ice
580 anomalies on the stratosphere. *Atmos. Chem. Phys.*, **12**, 11 819–11 831, doi:10.5194/acp-
581 12-11 819-2012.
- 582 Charlton, A. J. and L. M. Polvani, 2007: A new look at stratospheric sudden warmings.
583 Part I. Climatology and modeling benchmarks. *J. Clim.*, **20**, 449–469.
- 584 Charlton-Perez, A. J. and Coauthors, 2013: On the lack of stratospheric dynamical
585 variability in low-top versions of the CMIP5 models. *J. Geophys. Res. Atmos.*, **118**,
586 doi:10.1002/jgrd.50125.

587 Cohen, J., M. Barlow, P. J. Kushner, and K. Saito, 2007: Stratosphere-troposphere coupling
588 and links with Eurasian land surface variability. *J. Clim.*, **20**, 5335–5343.

589 Cohen, J., J. Foster, M. Barlow, K. Saito, and J. Jones, 2010: Winter 2009-2010: a
590 case study of an extreme Arctic Oscillation event. *Geophys. Res. Lett.*, **37**, L17707,
591 doi:10.1029/2010GL044256.

592 Cohen, J., et al., 2014: Recent Arctic amplification and extreme mid-latitude weather. *Nature*
593 *Geoscience*, **7(9)**, 627–637, doi:10.1038/ngeo2234.

594 Collins, M., et al., 2013: Long-term Climate Change: Projections, Commitments and Irre-
595 versibility. In: *Climate Change 2013: The Physical Science Basis. Contribution of Work-*
596 *ing Group I to the Fifth Assessment Report of the Intergovernmental Panel on Climate*
597 *Change*, [Stocker, T.F., D. Qin, G.-K. Plattner, M. Tignor, S. K. Allen, J. Boschung, A.
598 Nauels, Y. Xia, V. Bex and P.M. Midgley (eds.)]. Cambridge University Press, Cambridge,
599 United Kingdom and New York, NY, USA.

600 Deser, C., G. Magnusdottir, R. Saravanan, and A. Phillips, 2004: The effects of North
601 Atlantic SST and sea ice anomalies on the winter circulation in CCM3. Part II: direct and
602 indirect components of the response. *J. Clim.*, **17**, 877–889.

603 Domeisen, D. I. V., L. Sun, and G. Chen, 2013: The role of synoptic eddies
604 in the tropospheric response to stratospheric variability. *Geophys. Res. Lett.*, **40**,
605 doi:10.1002/grl.50943.

606 Edmon, H. J., B. J. Hoskins, and M. E. McIntyre, 1980: Eliassen-Palm cross sections for
607 the troposphere. *J. Atmos. Sci.*, **37**, 2600–2616.

608 Feldstein, S. and S. Lee, 2014: Intraseasonal and interdecadal jet shifts in the Northern
609 Hemisphere: The role of warm pool tropical convection and sea ice. *J. Clim.*, **27**, 6497–
610 6518.

611 Fletcher, C. G., S. C. Hardiman, P. J. Kushner, and J. Cohen, 2009: The dynamical response
612 to snow cover perturbations in a large ensemble of atmospheric GCM integrations. *J. Clim.*,
613 **22**, 1208–1222.

614 Garfinkel, C. I., D. L. Hartmann, and F. Sassi, 2010: Tropospheric precursors of anomalous
615 northern hemisphere stratospheric polar vortices. *J. Clim.*, **23**, 3282–3299.

616 Garfinkel, C. I., D. W. Waugh, and E. P. Gerber, 2013: The effect of tropospheric jet
617 latitude on coupling between the stratospheric polar vortex and the troposphere. *J. Clim.*,
618 **26**, 2077–2095.

619 Gerber, E. P. and Coauthors, 2010: Stratospheretroposphere coupling and annu-
620 lar mode variability in chemistryclimate models. *J. Geophys. Res.*, **115**, D00M06,
621 doi:10.1029/2009JD013770.

622 Gerber, E. P. and L. M. Polvani, 2009: Stratosphere-troposphere coupling in a relatively
623 simple AGCM: The importance of stratospheric variability. *J. Clim.*, **22**, 1920–1933.

624 Haynes, P. H., M. E. McIntyre, T. G. Shepherd, C. J. Marks, and K. P. Shine, 1991: On
625 the downward control of extratropical diabatic circulations by eddy-induced mean zonal
626 forces. *J. Atmos. Sci.*, **48**, 651–678.

627 Held, I. M. and M. J. Suarez, 1994: A proposal for the intercomparison of the dynamical
628 cores of atmospheric general circulation models. *Bull. Amer. Meteor. Soc.*, **75**, 1825–1830.

629 Jaiser, R., K. Dethloff, and D. Handorf, 2013: Stratospheric response to Arctic sea ice retreat
630 and associated planetary wave propagation changes. *Tellus A*, **65**.

631 Kim, B.-M., S.-W. Son, S.-K. Min, J.-H. Jeong, S.-J. Kim, X. Zhang, T. Shim, and J.-H.
632 Yoon, 2014: Weakening of the stratospheric polar vortex by Arctic sea-ice loss. *Nature*
633 *Communications*, **5**, doi:10.1038/ncomms5646.

634 Kushner, P. J. and L. M. Polvani, 2004: Stratosphere-troposphere coupling in a relatively
635 simple AGCM: The role of eddies. *J. Clim.*, **17**, 629–639.

636 Peings, Y. and G. Magnusdottir, 2014: Response of the wintertime Northern Hemisphere
637 atmospheric circulation to current and projected Arctic sea ice decline: a numerical study
638 with CAM5. *J. Clim.*, **27**, 244–264.

639 Pithan, F. and T. Mauritsen, 2014: Arctic amplification dominated by temperature feedbacks
640 in contemporary climate models. *Nature Geoscience*, **7**, 181–184,doi:10.1038/ngeo2071.

641 Polvani, L. M. and P. J. Kushner, 2002: Tropospheric response to stratospheric per-
642 turbations in a relatively simple general circulation model. *Geophys. Res. Lett.*, **29**,
643 10.1029/2001GL014284.

644 Polvani, L. M. and D. W. Waugh, 2004: Upward wave activity flux as precursor to extreme
645 stratospheric events and subsequent anomalous surface weather regimes. *J. Clim.*, **17**,
646 3548–3554.

647 Scinocca, J. F., M. C. Reader, D. A. Plummer, M. Sigmond, P. J. Kushner, T. G. Shepherd,
648 and A. R. Ravishankara, 2009: Impact of sudden Arctic sea-ice loss on stratospheric polar
649 ozone recovery. *Geophys. Res. Lett.*, **36**, L24701, doi:10.1029/2009GL041239.

650 Screen, J. A., I. Simmonds, C. Deser, and R. Tomas, 2013: The atmospheric response to
651 three decades of observed Arctic sea ice loss. *J. Clim.*, **26**, 1230–1248.

652 Simpson, I. R., P. Hitchcock, T. G. Shepherd, and J. F. Scinocca, 2011: Stratospheric
653 variability and tropospheric annular mode timescales. *Geophys. Res. Lett.*, **38**, L20806,
654 doi:10.1029/2011GL049304.

655 Simpson, I. R., P. Hitchcock, T. G. Shepherd, and J. F. Scinocca, 2013: Southern Annular
656 Mode dynamics in observations and models. Part 1: the influence of climatological zonal
657 wind biases in a comprehensive GCM. *J. Clim.*, **26**, 3953–3967.

- 658 Smith, K. L., C. G. Fletcher, and P. J. Kushner, 2010: The role of linear interference in the
659 Annular Mode response to extratropical surface forcings. *J. Clim.*, **23**, 6036–6050.
- 660 Sun, L., C. Deser, L. Polvani, and R. Tomas, 2014: The atmospheric response to three
661 decades of observed Arctic sea ice loss. *Environ. Res. Lett.*, **9**, 084016, doi:10.1088/1748–
662 9326/9/8/084016.
- 663 Sun, L., C. Deser, and R. A. Tomas, 2015: Mechanisms of stratospheric and tropospheric
664 circulation response to projected Arctic sea ice loss. *J. Clim.*, **28**, 7824–7845.
- 665 Wang, S., E. P. Gerber, and L. M. Polvani, 2012: Abrupt circulation responses to tropical
666 upper tropospheric warming in a relatively simple stratosphere-resolving AGCM. *J. Clim.*,
667 **25**, 4097–4115.

668 **List of Tables**

669 1 Details of the model experiments. Here we show the AA15 experiment as
670 an example; however, the details of all the experiments with other forcing
671 magnitudes are the same. 30

TABLE 1. Details of the model experiments. Here we show the AA15 experiment as an example; however, the details of all the experiments with other forcing magnitudes are the same.

Experiment Name	Description
CTRL	control experiment with Smith et al. (2010) model (or SFK10 model)
AA15	AA experiment with imposed AA-like thermal forcing as in Eq. (1) with $T_0^{AA} = 15$ K
NUDG AA15	nudging experiment by nudging the stratospheric zonal mean state towards that of the CTRL while imposing AA-like thermal forcing
NUDG downward-AA15	nudging experiment by nudging the stratospheric zonal mean state towards that of the AA15 and imposing no AA-like forcing
ZSYM E ^{strat}	zonally symmetric model experiment by applying the eddy forcing perturbation only in the stratosphere; the eddy forcing perturbation is computed in the AA15 experiment

672 List of Figures

- 673 1 Zonal mean temperature response [K] in the RCP8.5 scenario averaged across
674 30 CMIP5 models (shown in color shadings; thick black dashed-dotted line
675 denotes zero value). The anomaly is the average of November-December of
676 2080-2099 relative to 1980-1999 of historical runs. Thin black contours plot
677 T_{eq}^{AA} as in Equation (2) with $T_0^{AA} = 15$ K, $k = 5$, and $m = 3$. 34
- 678 2 (a) Zonal mean zonal wind in the control experiment in SFK10 model version;
679 (b)-(f) response of zonal mean zonal wind in AA5, AA10, AA15, AA20, and
680 AA25 experiment, respectively. The contour interval (CI) is 5 m/s in (a) with
681 black contours for positive values, gray contours for negative values, and thick
682 black contours for zero values. The CI is 1 m/s in (b)-(f) with red for positive
683 and blue for negative. The magenta contours plot T_{eq}^{AA} as in Eq. (2) with
684 CI = 2 K. The numbers on the north-west corner of the subplots in (b)-(f)
685 indicate the magnitude of AA, which is the near-surface temperature increase
686 poleward of 67.5°N in T_{eq}^{AA} . Statistically significant responses, at the 95%
687 level, are dotted. 35
- 688 3 Latitude (left) and intensity (right) of maximal zonal mean zonal wind for
689 the control and AA experiments at 841, 256, and 10 hPa. The results are
690 plotted in dashed-dotted lines for the control experiment and crosses for the
691 AA experiments with error bars showing two standard deviations. 36

692	4	(a) EP flux in the control experiment and (b) its response to AA15. The EP	
693		flux vectors are scaled according to Eq. (3.13) of Edmon et al. (1980) and	
694		the horizontal arrow scale, representing 10^{15} m^3 , is indicated in the upper-left	
695		corner of (a). The EP flux vectors in (b) are scaled by a factor of 20. The	
696		CI is 1 m/s/day in (a) and 0.2 m/s/day in (b). (c)-(f) Response in eddy	
697		meridional heat flux and its decomposition into the high frequency wave fluctu-	
698		ation term (FL), time-mean linear term (TM_{LIN}) and time-mean nonlinear	
699		term ($\text{TM}_{\text{NONLIN}}$). The CI is 0.5 K m/s in (c)-(f).	37
700	5	Similar to Fig. 2 but for zonal wind at 513 hPa. The CI is (a) 5 m/s, (b) 2	
701		m/s, and (c)-(f) 5 m/s.	38
702	6	SSW frequency in the control and AA experiments using (a) the standard	
703		method with reversal of westerly wind and (b) the NAM method. The results	
704		are plotted in dashed-dotted lines for the control experiment and crosses for	
705		the AA experiments with error bars showing the 2.5th and 97.5th percentiles	
706		using the bootstrapping method.	39
707	7	Eddy meridional heat flux (a) at 100 hPa and (b) averaged poleward of 45°N	
708		in the control and AA experiments.	40
709	8	NAM amplitude as a function of pressure levels in the control and NUDG AA	
710		experiments. See the text for details in the calculation of NAM amplitude.	41
711	9	(a)-(c) Zonal mean zonal wind in the control and AA15 experiments and their	
712		difference. (d) Zonal mean zonal wind in the NUDG AA15 experiment and	
713		(e) its change compared to control (can be considered as the response via the	
714		troposphere only). (f) The difference in zonal wind response between (c) and	
715		(e) (can be considered as the response via the stratospheric pathway only).	
716		(a) is the same as Fig. 2(a) and (c) is the same as Fig. 2(d). The CI is 5 m/s	
717		in (a)(b)(d) and 1 m/s in (c)(e)(f).	42

718	10	Zonal mean zonal wind response in NUDG downward-AA15 experiment (a)	
719		and in the zonally symmetric model configuration with the eddy forcing per-	
720		turbation confined to the stratosphere, E^{strat} (b). The CI is 1 m/s in (a)(b).	43
721	11	Similar to Fig. 3 but including the results in NUDG experiments, plotted in	
722		red crosses and error bars.	44
723	12	Similar to Fig. 9 but using the GP09 model version with a tropospheric jet	
724		located near 42°N.	45

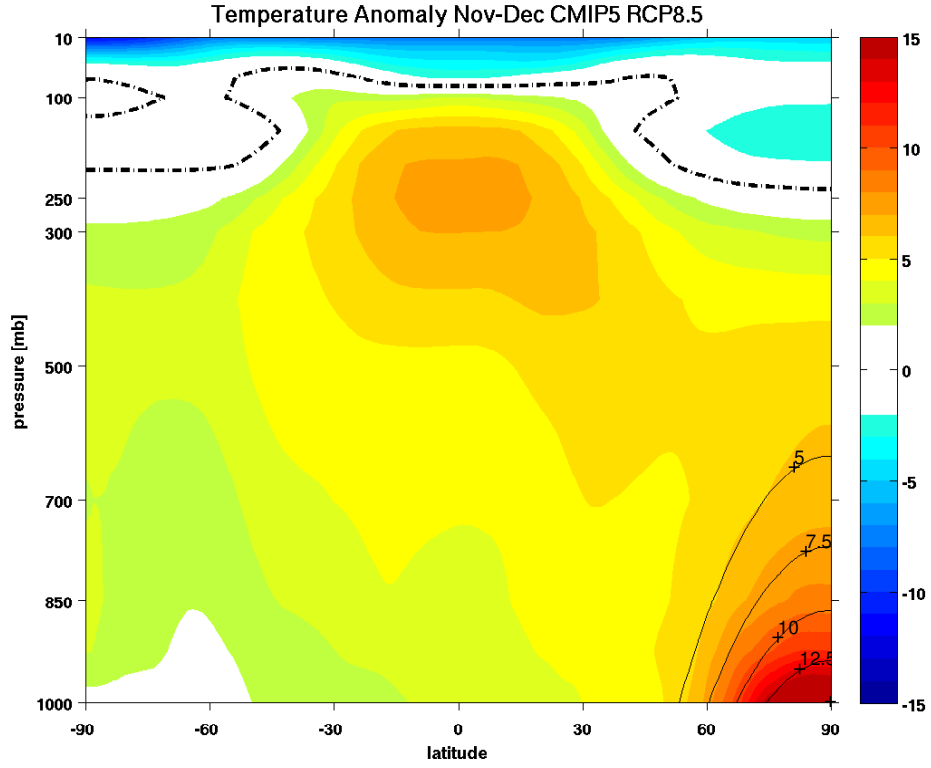


FIG. 1. Zonal mean temperature response [K] in the RCP8.5 scenario averaged across 30 CMIP5 models (shown in color shadings; thick black dashed-dotted line denotes zero value). The anomaly is the average of November-December of 2080-2099 relative to 1980-1999 of historical runs. Thin black contours plot T_{eq}^{AA} as in Equation (2) with $T_0^{AA} = 15$ K, $k = 5$, and $m = 3$.

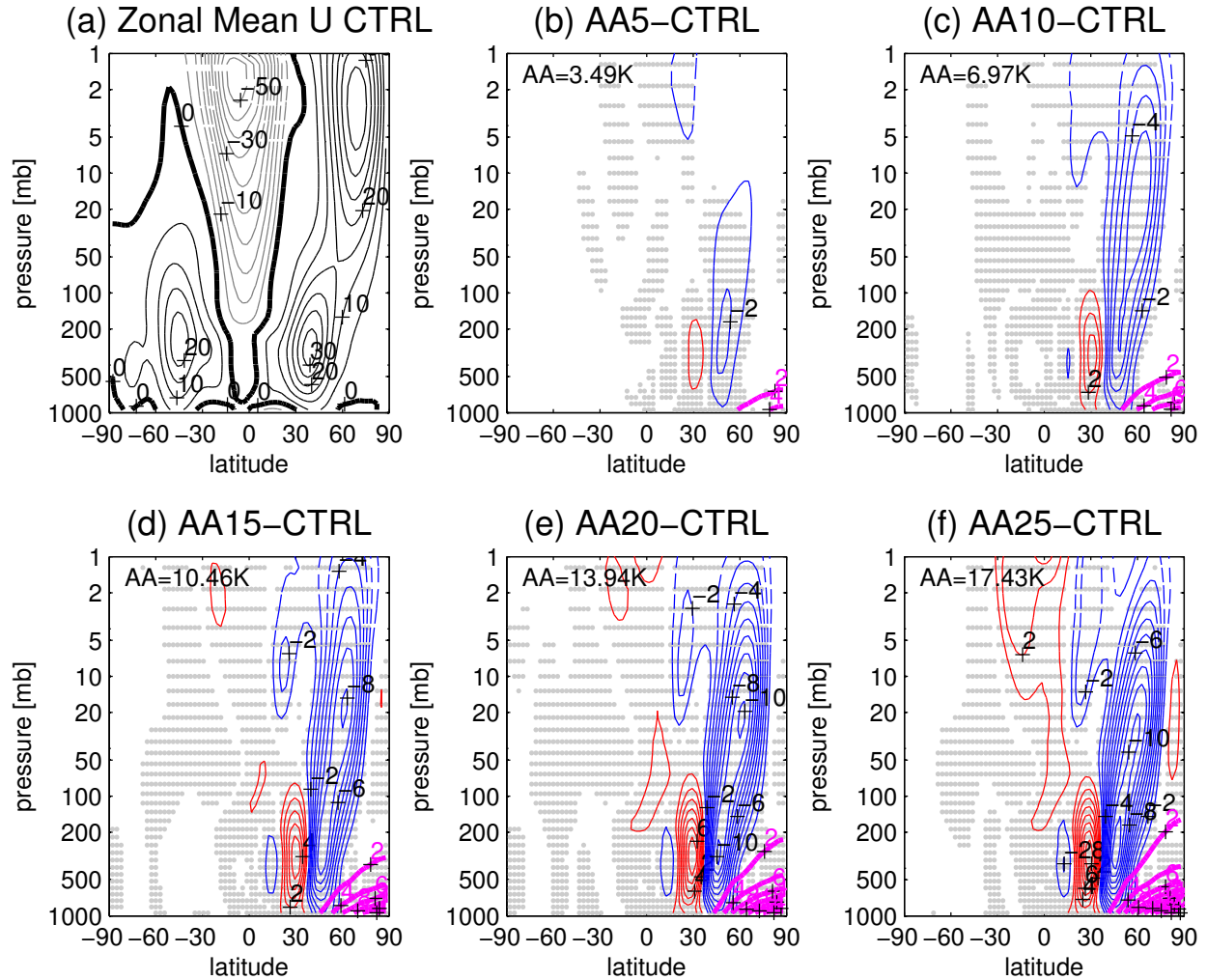


FIG. 2. (a) Zonal mean zonal wind in the control experiment in SFK10 model version; (b)-(f) response of zonal mean zonal wind in AA5, AA10, AA15, AA20, and AA25 experiment, respectively. The contour interval (CI) is 5 m/s in (a) with black contours for positive values, gray contours for negative values, and thick black contours for zero values. The CI is 1 m/s in (b)-(f) with red for positive and blue for negative. The magenta contours plot T_{eq}^{AA} as in Eq. (2) with CI = 2 K. The numbers on the north-west corner of the subplots in (b)-(f) indicate the magnitude of AA, which is the near-surface temperature increase poleward of 67.5°N in T_{eq}^{AA} . Statistically significant responses, at the 95% level, are dotted.

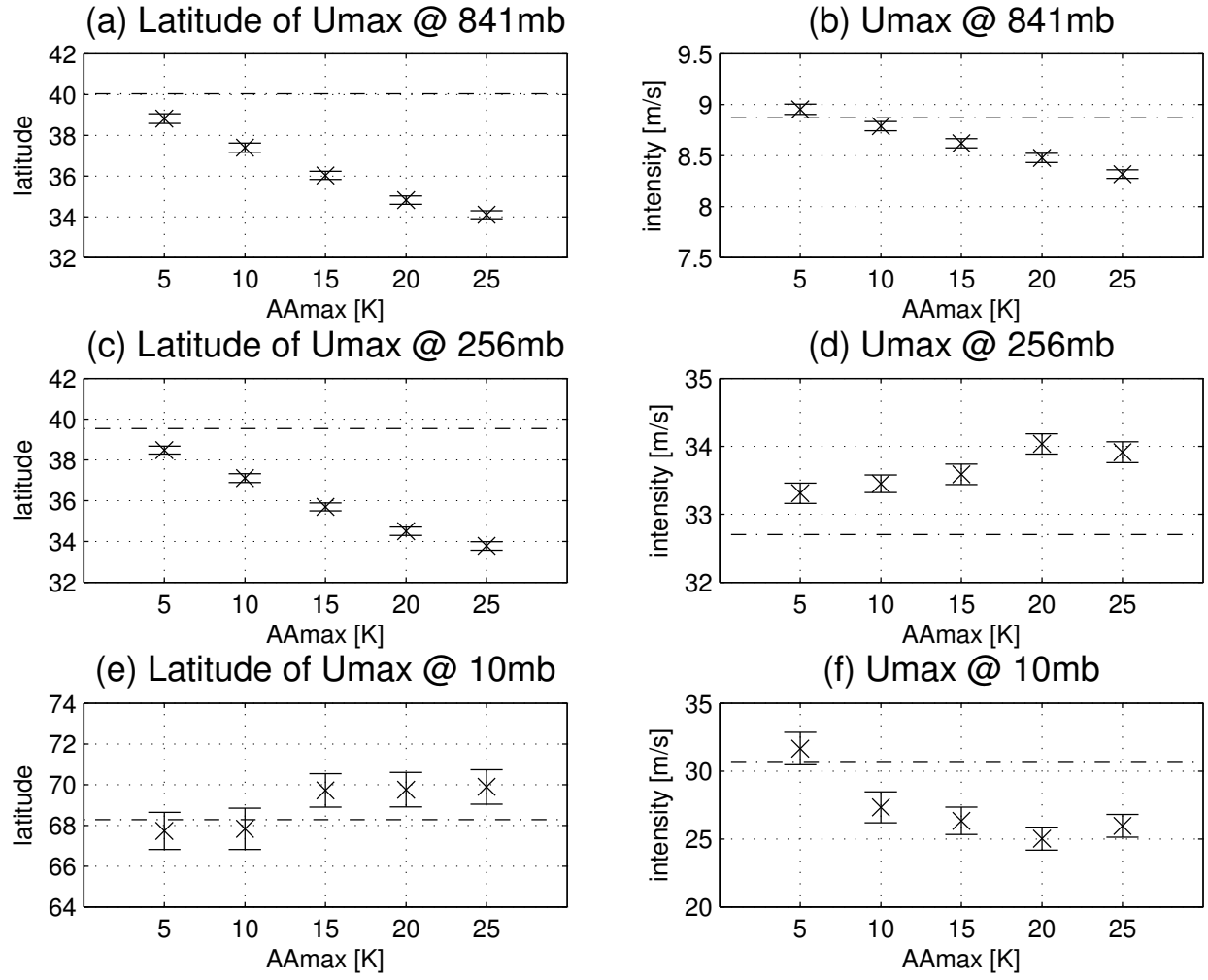


FIG. 3. Latitude (left) and intensity (right) of maximal zonal mean zonal wind for the control and AA experiments at 841, 256, and 10 hPa. The results are plotted in dashed-dotted lines for the control experiment and crosses for the AA experiments with error bars showing two standard deviations.

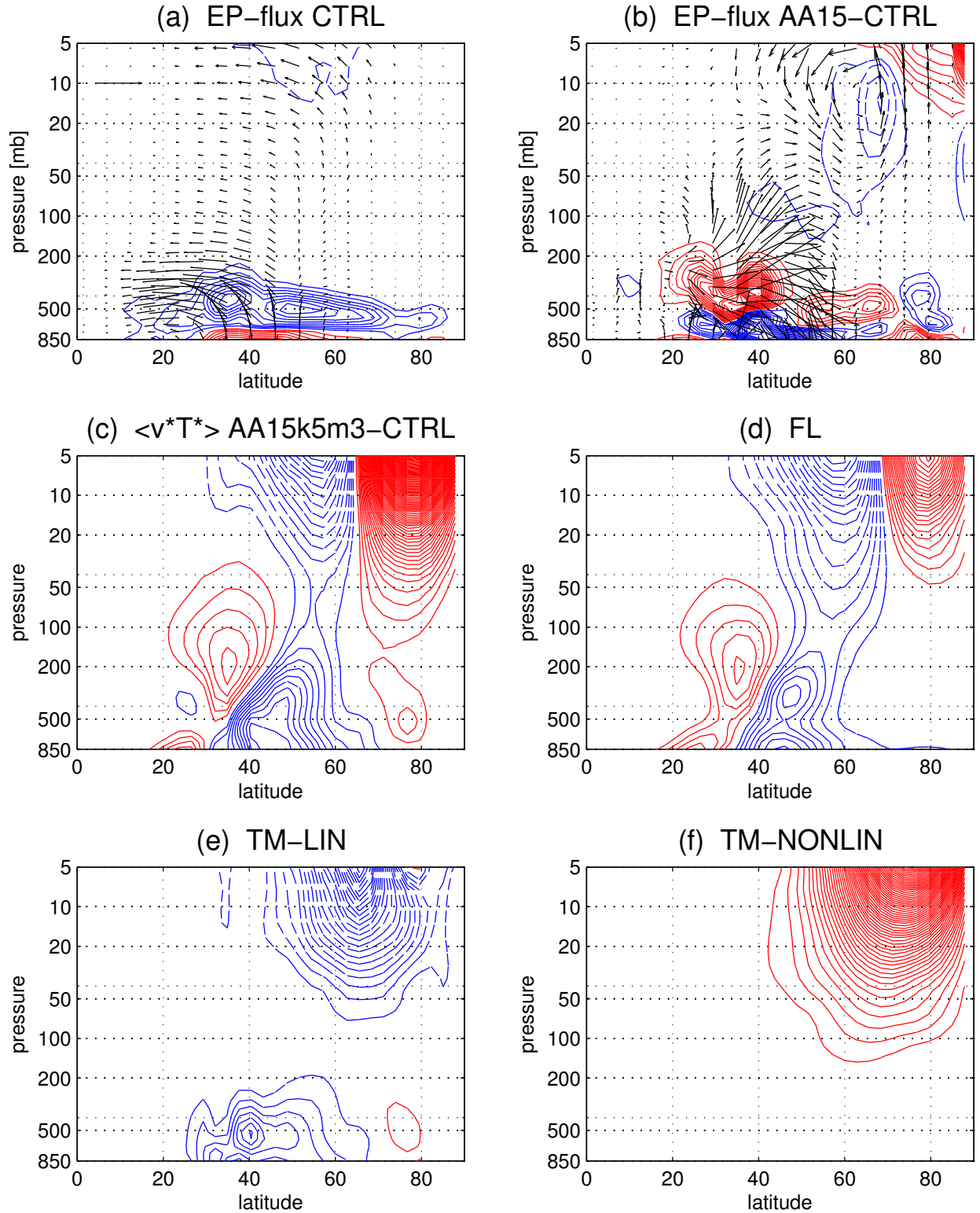


FIG. 4. (a) EP flux in the control experiment and (b) its response to AA15. The EP flux vectors are scaled according to Eq. (3.13) of Edmon et al. (1980) and the horizontal arrow scale, representing 10^{15} m^3 , is indicated in the upper-left corner of (a). The EP flux vectors in (b) are scaled by a factor of 20. The CI is 1 m/s/day in (a) and 0.2 m/s/day in (b). (c)-(f) Response in eddy meridional heat flux and its decomposition into the high frequency wave fluctuation term (FL), time-mean linear³⁷ term (TM_{LIN}) and time-mean nonlinear term (TM_{NONLIN}). The CI is 0.5 K m/s in (c)-(f).

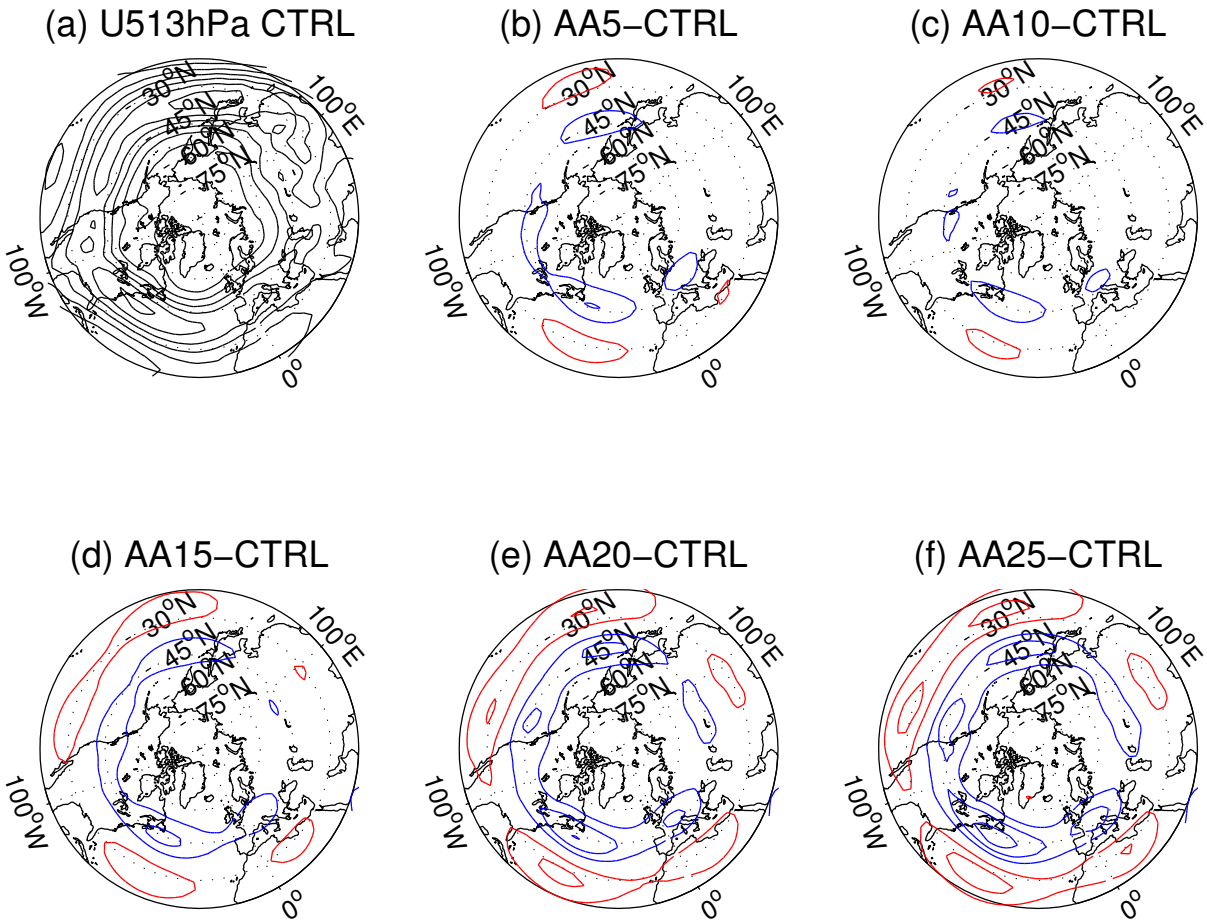


FIG. 5. Similar to Fig. 2 but for zonal wind at 513 hPa. The CI is (a) 5 m/s, (b) 2 m/s, and (c)-(f) 5 m/s.

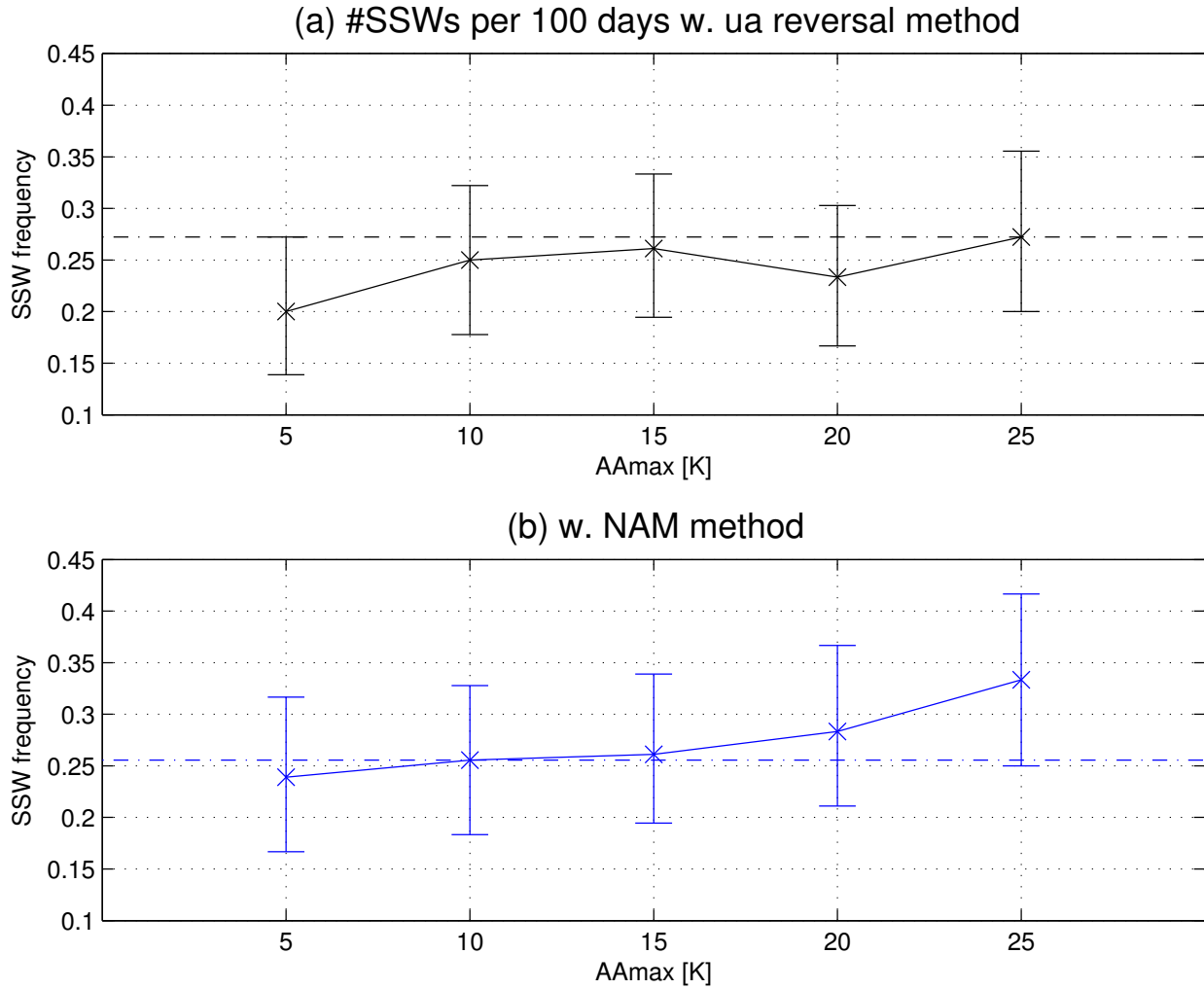


FIG. 6. SSW frequency in the control and AA experiments using (a) the standard method with reversal of westerly wind and (b) the NAM method. The results are plotted in dashed-dotted lines for the control experiment and crosses for the AA experiments with error bars showing the 2.5th and 97.5th percentiles using the bootstrapping method.

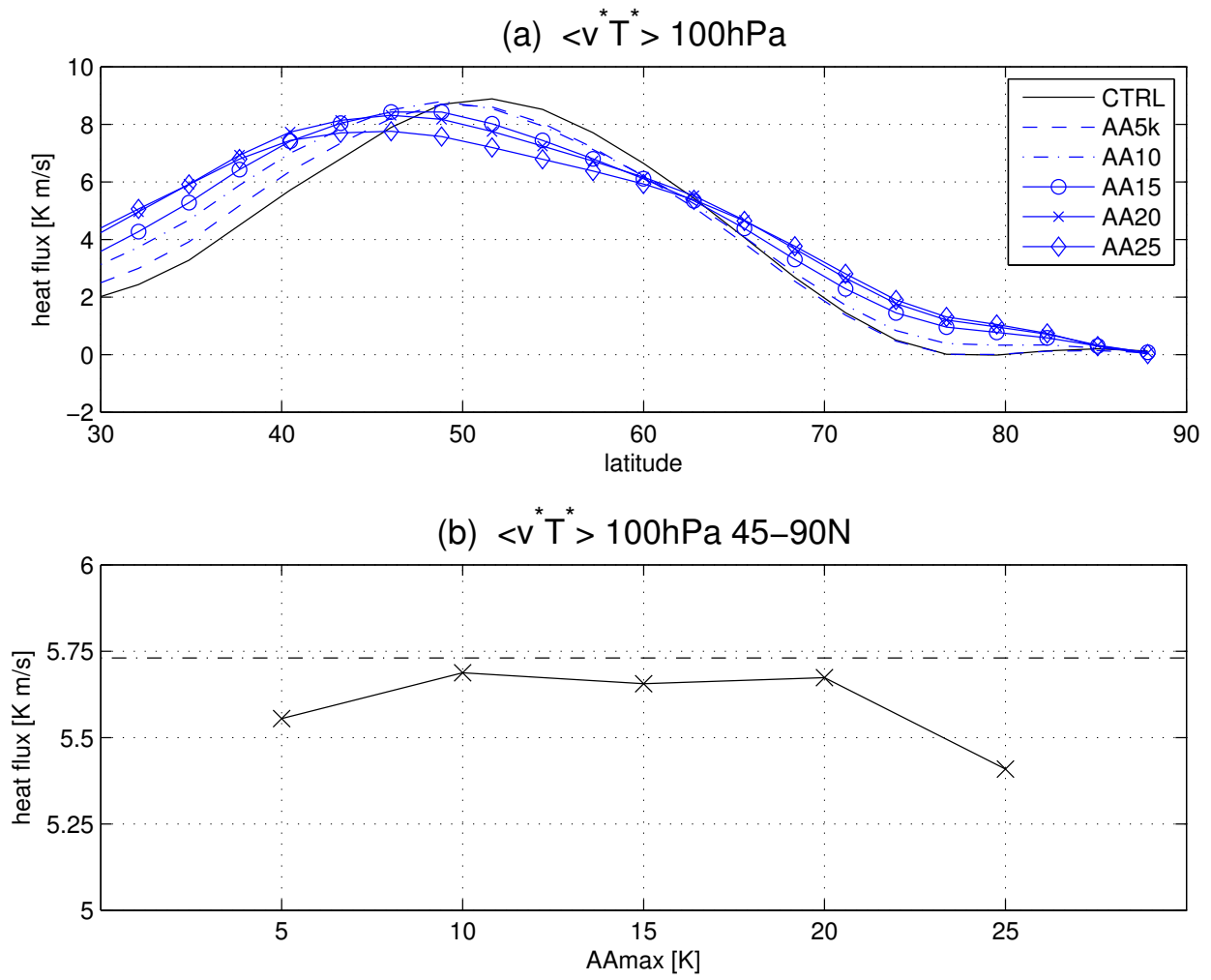


FIG. 7. Eddy meridional heat flux (a) at 100 hPa and (b) averaged poleward of 45°N in the control and AA experiments.

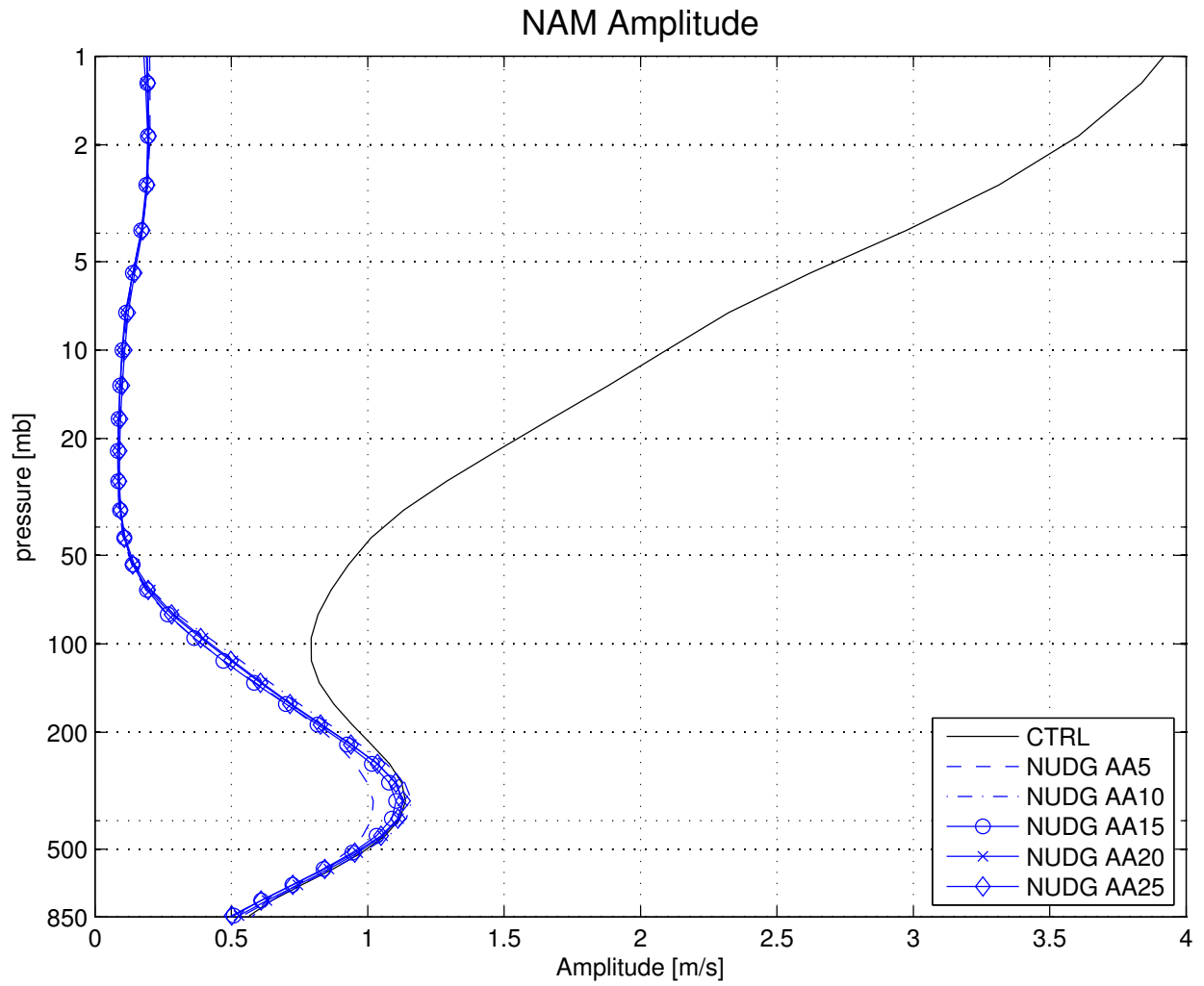


FIG. 8. NAM amplitude as a function of pressure levels in the control and NUDG AA experiments. See the text for details in the calculation of NAM amplitude.

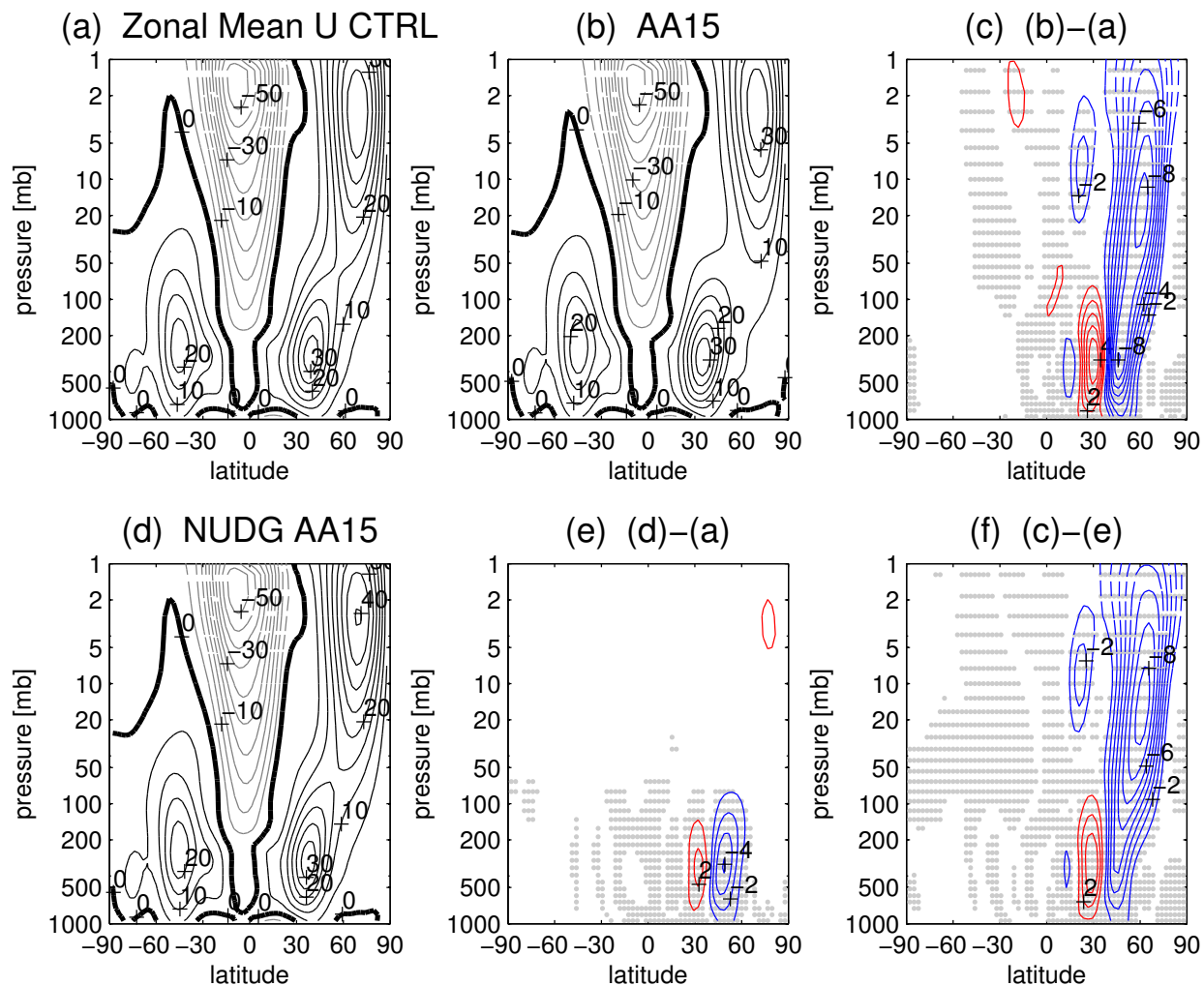


FIG. 9. (a)-(c) Zonal mean zonal wind in the control and AA15 experiments and their difference. (d) Zonal mean zonal wind in the NUDG AA15 experiment and (e) its change compared to control (can be considered as the response via the troposphere only). (f) The difference in zonal wind response between (c) and (e) (can be considered as the response via the stratospheric pathway only). (a) is the same as Fig. 2(a) and (c) is the same as Fig. 2(d). The CI is 5 m/s in (a)(b)(d) and 1 m/s in (c)(e)(f).

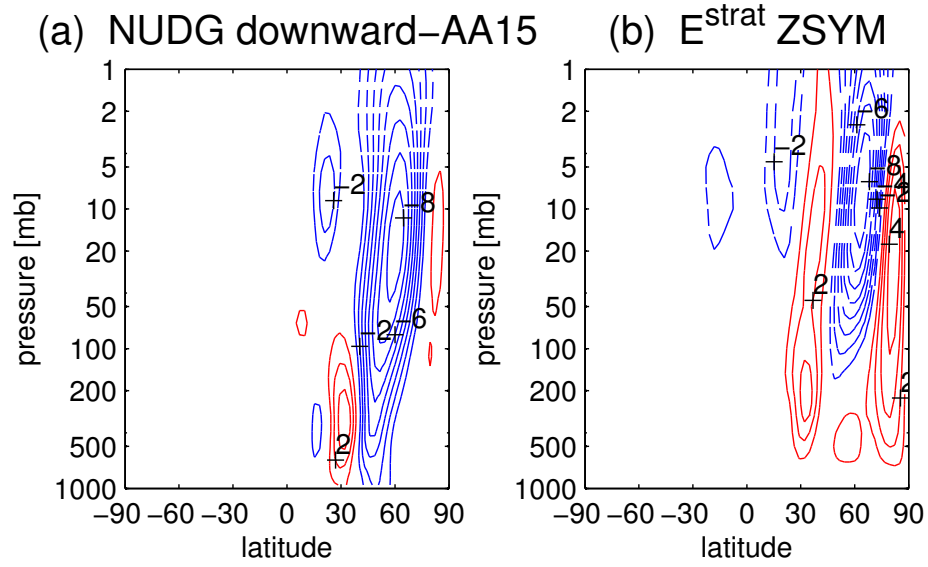


FIG. 10. Zonal mean zonal wind response in NUDG downward-AA15 experiment (a) and in the zonally symmetric model configuration with the eddy forcing perturbation confined to the stratosphere, E^{strat} (b). The CI is 1 m/s in (a)(b).

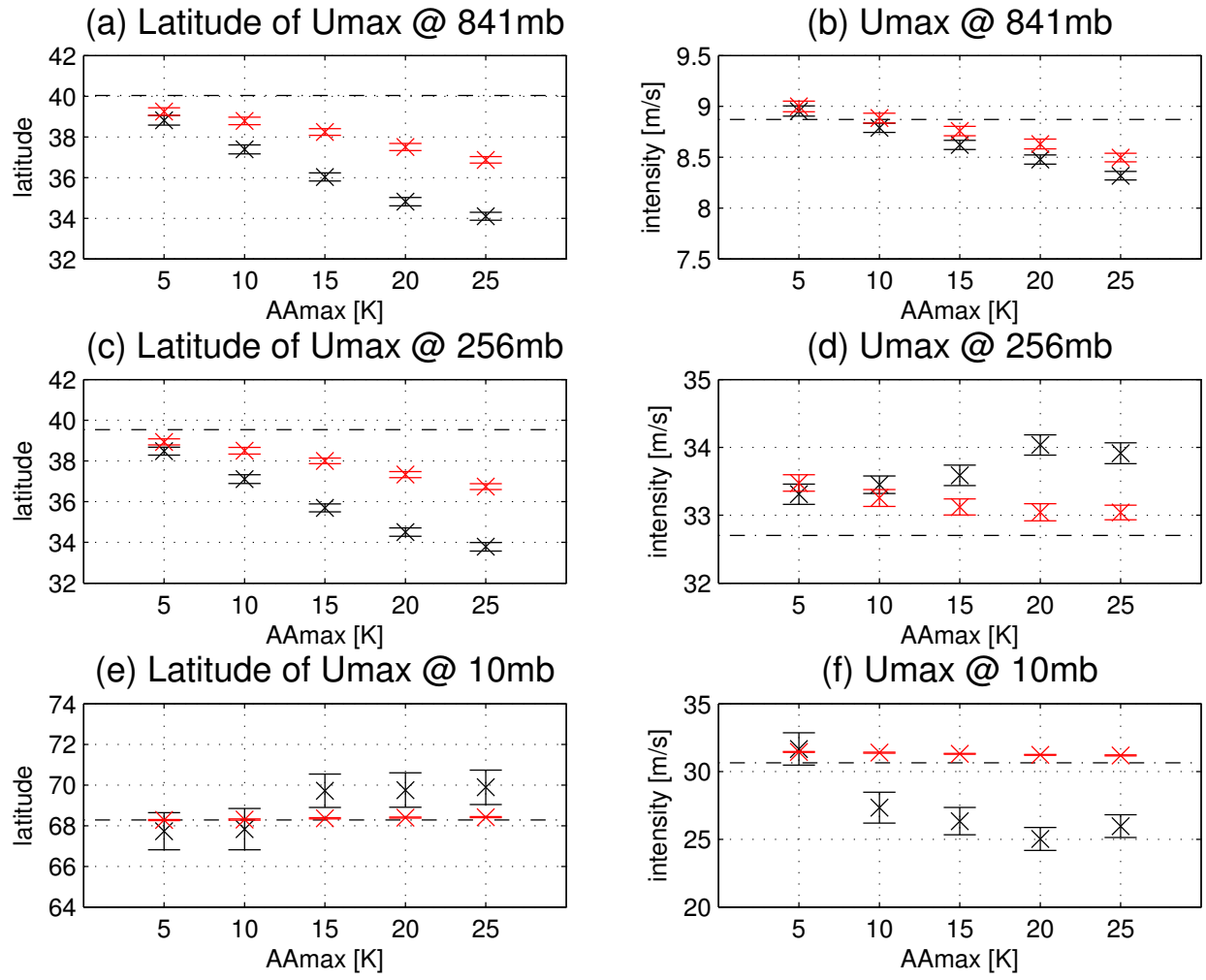


FIG. 11. Similar to Fig. 3 but including the results in NUDG experiments, plotted in red crosses and error bars.

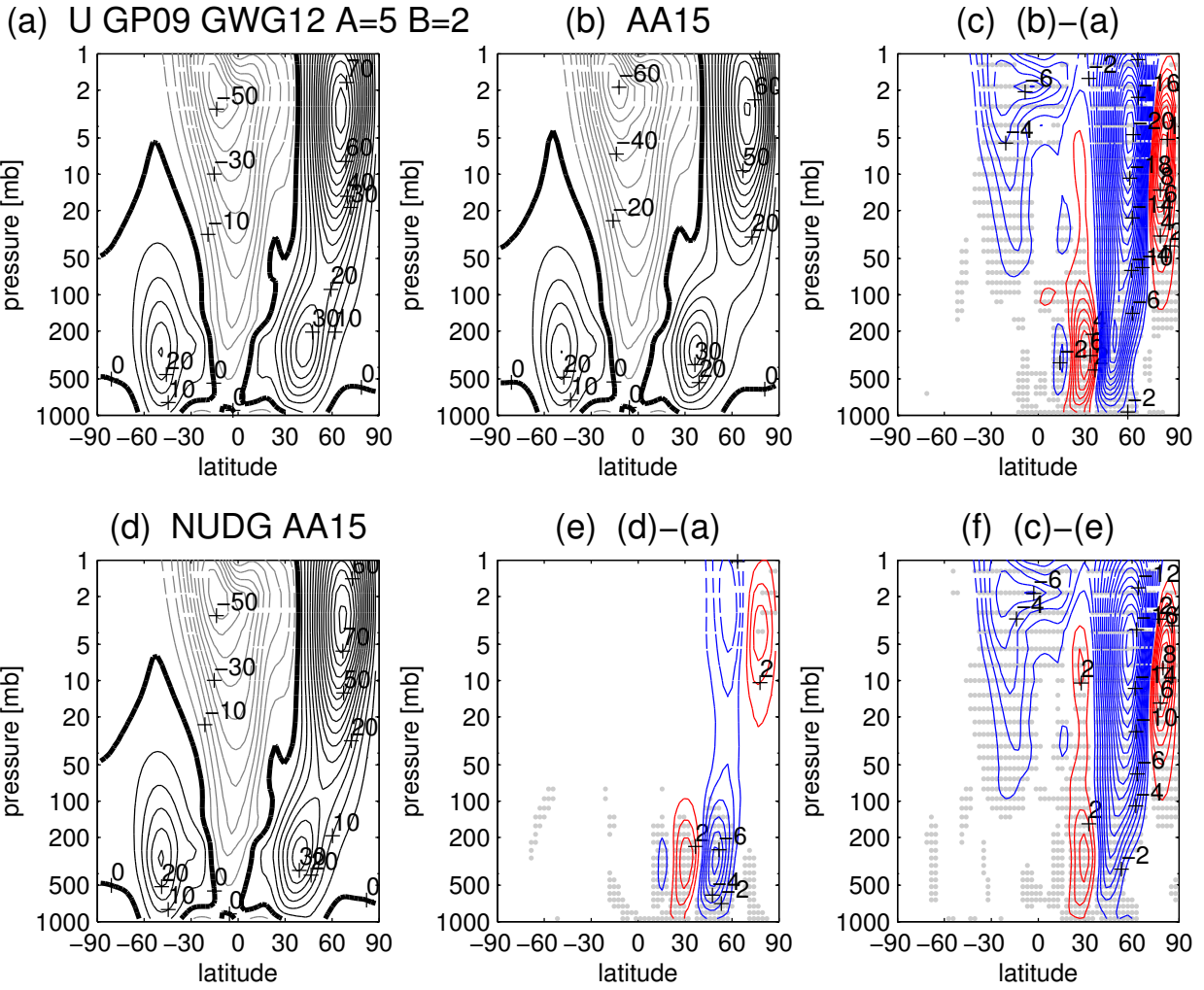


FIG. 12. Similar to Fig. 9 but using the GP09 model version with a tropospheric jet located near 42°N.